Investigation to charge cooling effect and combustion characteristics of ethanol direct injection in a gasoline port injection engine

Yuhan Huang [a,b *], Guang Hong [a], Ronghua Huang [b]

Affiliations:

[a] School of Electrical, Mechanical and Mechatronic Systems, University of Technology Sydney, Sydney, Australia

[b] State Key Laboratory of Coal Combustion, Huazhong University of Science and Technology, Wuhan, China

Corresponding author:

Yuhan Huang, BE

Postal address: School of Electrical, Mechanical and Mechatronic Systems, University of Technology Sydney, PO Box 123, Broadway NSW 2007, Australia

Email: Yuhan.Huang@student.uts.edu.au

Telephone: +61 415040942

Abstract

Ethanol direct injection has the potentials to increase the engine compression ratio and thermal efficiency by taking advantages of ethanol fuel such as the high octane number and latent heat. In this study, CFD modelling and experiments were carried out to investigate the charge cooling effect and combustion characteristics of ethanol direct injection in a gasoline port injection (EDI+GPI) engine. Experiments were conducted on a single-cylinder spark ignition engine equipped with EDI+GPI over a full range of ethanol ratio from 0% (GPI only) to 100% (EDI only). Multidimensional CFD simulations to the partially premixed dual-fuel spray combustion were performed to understand the experimental results. The simulations were verified by comparing with the experimental results. Simulation results showed that the overall cooling effect of EDI was enhanced with the increase of ethanol ratio from 0% to 58%, but was not enhanced with further increase of ethanol ratio. When the ethanol ratio was greater than 58%, a large number of liquid ethanol droplets were left in the combustion chamber during combustion and fuel impingement on the cylinder wall became significant, leading to local overcooling in the near-wall region and over-lean mixture at the spark plug gap. As a consequence, the CO and HC emissions increased due to incomplete combustion. Compared with GPI only, the faster flame speed of ethanol fuel contributed to the greater peak cylinder pressure of EDI+GPI condition, which resulted in higher power output and thermal efficiency. Meanwhile, the mixture became leaner with the increase of ethanol ratio. As a result, the IMEP was increased, combustion initiation duration and major combustion duration were decreased when ethanol ratio was in 0%-58%. The combustion performance was deteriorated when ethanol ratio was greater than 58%. Experimental and numerical results showed

that the IMEP, thermal efficiency and emissions of this EDI+GPI engine can be optimized in the range of ethanol ratio of 40-60%.

Keywords:

Ethanol direct injection; Gasoline port injection; CFD modelling; Cooling effect; Combustion characteristics

1. Introduction

Engine downsizing is a promising technology to achieve the future CO_2 reduction target of spark ignition (SI) engines [1-4]. However one major issue associated with the downsized engines is the increased knock propensity [1, 4]. Recently ethanol direct injection (EDI) has emerged as a potential technology to fully implement the engine downsizing. The engine knock propensity can be reduced by the higher octane number of ethanol fuel, and supplemented by the cooling effect enhanced by direct injection and ethanol's greater latent heat.

Compared with port injection (PI), direct injection (DI) is more effective for charge cooling due to fuel evaporation inside the combustion chamber. Moreover, cooling effect of DI can be further enhanced by the fuel with greater latent heat of vaporization, such as ethanol fuel. Cooling effect of DI has been measured in different ways. The most effective way may be to measure the in-cylinder temperature directly. Kar et al. [5] and Price et al. [6] used a cold wire resistance thermometer to measure the in-cylinder temperature in PI and DI engines. However this method requires fast response of the temperature sensor and protection for the fragile sensor. So the measurements were only performed in non-firing conditions [5, 6]. The Planar Laser Induced Fluorescence (PLIF) thermometry technique was used to measure the cylinder temperature of DI engines [7]. Up to date, the experimental methods to quantify the charge cooling used the parameters linked to the charge cooling directly or indirectly, such as in-cylinder pressure, volumetric efficiency, anti-knock ability, etc. Ahn et al. [8] used in-cylinder pressure to evaluate the cooling effect of ethanol fuel. Wyszynski et al. [9] measured the volumetric efficiency of different fuels on a DI SI engine fitted with both port and direct fuel injection systems. However, using intake air flow rate to quantify the amount of charge cooling only captured part of the cooling effect that took place during the intake stroke. Fuel evaporation process may continue after the intake valves are closed, and even in the combustion process [10]. To evaluate the cooling effect on a special aim, knock onset was used to measure the charge cooling effect in a turbocharged SI engine equipped with both PI and DI of blended ethanol/gasoline fuels [10, 11]. Similar investigation was carried out in an attempt to identify the thermal and chemical benefits of DI and PI [12]. They reached the same conclusion that the ethanol's cooling effect enhancement to the engine performance was comparable to that of its higher Octane number [11, 12]. To quantify the thermal and chemical benefits of ethanol fuel, it is reported that a 2-8 kJ/kg increase of "cooling power" of the mixture had the same impact as one-point increase of research octane number (RON) [1]. Or 10% of ethanol addition to gasoline results in five-point increase of RON [13].

Meanwhile, numerical simulations have also been applied to investigate the cooling effect. 0-D simulations (involving no engine geometry) were performed to calculate the theoretical improvement in volumetric efficiency of DI over PI [9]. 1-D gas dynamics and thermodynamics engine simulations were carried out to investigate the anti-knock effect of direct injection with ethanol/gasoline blends [11]. As the 0-D and 1-D simulations were developed for special purposes, the information obtained in the results was limited. Kasseris et al. [10] used 3-D numerical modelling to investigate the effect of intake air temperature on the amount of realized charge cooling. The simulation results showed that almost all the theoretical charge cooling was realized when the intake air temperature was increased to 120 ℃. However the simulated evaporation rate of ethanol fuel in low temperature conditions (naturally aspirated engines) was much lower than gasoline’s [14, 15]. This limited the cooling effect of ethanol fuel.

Since ethanol has high latent heat and low evaporation rate, EDI is not appropriate to be used on SI engines alone in cold conditions (e.g. cold start problem) [14]. One alternative way is to use it with gasoline port injection (GPI). Studies have investigated the dual-injection concept. The dual-injection concept for knock mitigation with E85 DI plus gasoline PI was tested [16]. The combustion characteristics of three different dual-injection strategies, including gasoline PI plus gasoline DI, gasoline PI plus E85 DI, and E85 PI plus gasoline DI, were investigated [17]. The dual-injection concept of gasoline PI and ethanol or DMF DI was studied as a flexible way to use bio-fuels [18]. The knock mitigation ability [19] and combustion characteristics [20] of dual-injection strategy were examined. The leveraging effect and knock mitigation of EDI in a GPI SI engine (EDI+GPI) were investigated recently [21, 22].

The above reviewed experimental studies have shown advantages of EDI+GPI over the conventional PI engines. The thermal efficiency was improved [16-18, 21] and knock propensity was reduced [16, 19, 22], while some reported the increase of HC, CO [21, 22] or NO emissions [19] when EDI was applied. Although experimental investigations are reliable and essential in the development of EDI+GPI engine, they are costly and difficult to understand the in-cylinder mixture formation and combustion mechanisms of this new combustion system. Nowadays, multi-dimensional computational fluid dynamics (CFD) modelling has been proven a useful tool to exploit the detailed and visualised information about the in-cylinder flows. The dual-fuel combustion of in-cylinder fuel blending by gasoline port injection and early diesel direct injection was modelled with a 60 degree sector mesh of the combustion chamber [23]. The combustion and emission characteristics of a dual-fuel injection system with gasoline port injection and diesel direct injection were numerically investigated with a 45 degree sector mesh [24]. However, since the computational meshes used in refs. [23, 24] did not include the intake manifold, the gasoline port injection spray was not modelled. The dual-fuel combustion with diesel direct injection and natural gas premixed with air in the intake manifold was simulated [25]. CFD modelling was conducted to investigate the spray, mixture preparation and combustion processes in a spray-guided DI SI engine [26]. CFD models coupled with detailed chemical reaction mechanisms were applied to simulate the multi-component fuel spray combustion [27, 28]. However, coupling the chemistry with the CFD solver is very time consuming and incompatible for complex industrial configurations [29, 30]. Instead, Extended Coherent Flame Model (ECFM) was adopted to simulate the combustion process of SI engines [29, 31, 32]. To accommodate the increasingly complex chemical kinetics, realistic turbulence/chemistry interaction and multiple combustion regimes in three-dimensional time-dependent device-scale CFD modelling is a difficult task in turbulent combustion [33]. A hybrid approach of probability density function (PDF) method and laminar flamelet model was applied to address the issue [33]. To reduce the computational cost, the complex reaction mechanisms can be pre-computed and stored in look-up tables [30, 34]. The ECFM combined with PDF look-up tables were used to model the turbulent diesel spray flames [35, 36]. A presumed PDF model was applied to predict the turbulent flow behavior and temperature distribution of a diesel spray combustion flame [37]. A tabulated chemistry method was developed to investigate turbulence-chemistry interactions of premixed, non-premixed and partially premixed flames [30]. By reviewing the above numerical studies, few publication was found on studying the cooling effect and spray combustion of dual-injection engine. Moreover simultaneously tracking the evaporation and combustion processes of two fuels is challenging and computationally consuming.

In this study, the cooling effect and combustion characteristics of a novel fuel system, ethanol direct injection plus gasoline port injection (EDI+GPI), were numerically and experimentally investigated in a full range of ethanol ratio from 0% (GPI only) to 100% (EDI only).

Nomenclature		IMEP	Indicated mean effective pressure
ASOI	After the start of injection	MFB	Mass fraction burnt
BTDC	Before top dead centre	PDF	Probability density function
CAD	Crank angle degrees	PI	Port injection
CFD	Computational fluid dynamics	RON	Research octane number
DI	Direct injection	SI	Spark ignition
ECFM	Extended Coherent Flame Model	Φ	Equivalence ratio
EDI	Ethanol direct injection	CA0-10%	Combustion initiation duration
GPI	Gasoline port injection	CA10-90%	Major combustion duration
EDI+GPI	Ethanol direct injection plus gasoline port injection	E'X'	X% ethanol by volume. e.g. E46 is 46% ethanol via DI + 54% gasoline via PI

2. Experimental setup

2.1. EDI+GPI engine

Fig. 1 shows the schematic of the EDI+GPI research engine and Table 1 gives the engine specifications. The engine was modified from a single cylinder, four-stroke, air-cooled SI engine which was used on the Yamaha YBR250 motorcycle. It was modified to EDI+GPI engine by adding an EDI fuel system to the engine. The EDI injector was a six-hole injector with a spray angle of 34° and a bent angle of 17°. The EDI injector was mounted with spray plumes bent towards the spark plug to create an ignitable mixture around the spark plug. Both the GPI injector and EDI injector were controlled by an electronic control unit. The EDI+GPI fuel system offers the flexibility to operate the engine over a full range of ethanol ratio from 0% (GPI only) to 100% (EDI only). The cylinder pressure, engine torque, intake and exhaust temperatures, cylinder head temperature and emissions were measured during the experiments, which provided experimental data for engine modelling. More information about the engine test system and EDI injector can be found in [21, 38].

2.2. Engine operating conditions

Table 2 lists the tested engine conditions in the present study. The engine was run at 4000 rpm and 36% throttle open which was the medium engine load in [21]. The lambda was monitored and kept around one by adjusting the mass flow rates of the gasoline and ethanol fuels at a designated fuel ratio and a fixed throttle position. Horiba MEXA-584L gas analyser can measure the lambda of multiple fuels with atomic ratios of hydrogen to carbon (H/C) and oxygen to carbon (O/C) of the fuel input by the user. To ensure the accuracy and correction of the lambda value, the lambda measured by the Horiba gas analyser was also compared with the one calculated using the mass flow rates of the gasoline fuel, the ethanol fuel and the intake air. The intake air flow rate was measured by a ToCeil20N hot-wire thermal air-mass flow meter. The gasoline and ethanol fuel flow rates were determined by the injection pulse width of the injectors in the engine control unit. The fuel injectors were calibrated by the Hents Technologies Inc. at various injection pressures and pulse widths. A linear function between the injector's pulse width and fuel mass was derived from the calibration results. The calibration of fuel mass and pulse width has shown good and stable linearity at different injection pressures. The EDI injection timing was 300 CAD BTDC and the GPI timing was 410 CAD BTDC. EDI timing of 300 CAD BTDC was for providing sufficient time for ethanol fuel to evaporate and to mix with air before the combustion took place. The spark timing was 15 CAD BTDC which was the spark timing in the original engine control system. The EDI pressure was 6.0 MPa and the GPI pressure was 0.25 MPa. The ethanol ratio was varied from 0% (GPI only) to 100% (EDI only), including E0, E25, E46, E58, E69, E76, E85 and E100 (E'X' means X% ethanol by volume. e.g. E46 is 46% ethanol via DI + 54% gasoline via PI).

3. Computational models

3.1. Dual-fuel spray combustion modelling

The numerical simulations were performed with the CFD code ANSYS FLUENT. The in-cylinder flows were modelled using the RANS based realizable k-ε turbulence model. The EDI and GPI sprays were simulated by the Discrete Droplet Model (DDM) based on the Eulerian-Lagrangian approach. A set of sub-models were adopted to take into account the effects of break-up, fuel evaporation, droplet-gas momentum exchange, and droplet-wall interaction. The primary breakup process is modelled by the Rosin-Rammler Diameter Distribution Method based on the blob injection concept which assumes the initial droplets or blobs to be similar to the injector hole diameter at the nozzle exit [39-42]. The consequent droplet breakup process was modelled by the WAVE model [43]. Dynamic Drag model was used to take into account the droplets distortion and drag [44]. Since the simulated cases were completely warmed up engine conditions, the cylinder wall was hot and the Wall-jet model was adopted to model the droplet-wall interactions [45]. Convection/Diffusion Controlled Model [46] was adopted to model the evaporation process of ethanol and gasoline droplets. It uses the vapour pressure as the driving force for droplets evaporation and incorporates the effect of the convective flow on the evaporating materials from the droplet surface to the bulk gas phase. The evaporation model provided the combustion model with the amount of vapour fuel for each fuel.

Spray combustion in SI engines is a typical partially premixed combustion which shows features of both non-premixed and premixed combustion. The fuel is injected into the combustion chamber in liquid form and evaporation and diffusion processes occur prior to the combustion. By the time of combustion, part of the fuel has mixed with the oxidizer in molecular level but inhomogeneously, and evaporating and mixing are still occurring. The dual-fuel spray combustion process was modelled using the ECFM combustion model with the partially premixed combustion concept in which both the mixture fraction Z and progress variable c were solved [29, 45, 47]. The combustion process was initiated by releasing a specific amount of energy to the cells at the spark plug gap at the spark timing. The presumed PDF look-up table was used to model the turbulence-chemistry interactions. The chemistry look-up tables were generated using complex reaction mechanisms which incorporated the latest insights on combustion chemical kinetics [34]. For single fuel combustion modelling (GPI only and EDI only conditions), a three-dimensional PDF table was generated to determine the temperature, density, and species fraction in the turbulent flame. For EDI+GPI dual-fuel combustion modelling, a five-dimensional PDF table was generated to take into account the secondary fuel. The computational cost of implementing five-dimensional PDF table was much higher than three-dimensional one. The thermal NO formation was modelled by the extended Zeldovich mechanism [29].

3.2. Computational mesh

The computational mesh was generated based on the scanned geometry of the cylinder head using the ANSYS Meshing. Fig. 2 shows the computational mesh at the start of the calculation. It mainly consists of tetrahedral grids. However the regions with moving boundaries were meshed to hexahedral grids for mesh deforming. A basic requirement for the Lagrangian liquid phase description is that the void fraction within a cell is close to one [48]. To meet this requirement, the grid sizes near the nozzles are at least five times larger than the nozzle diameters [28, 49]. An earlier study by the current authors [50] showed that the present mesh was sufficient to achieve the reasonable accuracy and low computational cost. More details about the dynamic mesh and independence study can be found in [50].

3.3. Boundary and initial conditions

The boundary and initial conditions were determined according to the experimental conditions described in Section 2.2. The wall temperatures were set up based on the typical temperature distributions for SI engines operating at normal steady state conditions [51]. The wall temperatures were set to be 600 K for the cylinder head, 458 K for the cylinder linear, 573 K for the piston, 523 K for the intake valve, and 923 K for the exhaust valve. The wall temperatures of intake and exhaust ports are assumed to be 333 K and 723 K respectively. The inlet and outlet pressure values were constant as the atmospheric pressure. The intake air temperature was set to be the room temperature of the engine laboratory. Initial conditions for the cylinder, intake and exhaust manifolds were set up according to the measured in-cylinder pressure and exhaust gas temperature.

3.4. Comparison between measured and simulated results

The comparison between the measured and simulated values of in-cylinder pressure and heat release rate at different ethanol ratios are shown in Fig. 3. As shown in Fig. 3, the simulated cylinder pressure and heat release rate, including their magnitudes and phases, agree well with the measured data from the engine experiments. As the ethanol ratio increases to E76, the simulated in-cylinder pressure increases slightly more quickly than the measured one does after the spark timing. However, the start phase and the magnitude of the heat release rate of the simulated curve still match with the measured one at E76. Therefore, the accuracy of the simulation is considered within the acceptable limit considering the current development of dual-fuel combustion modelling.

4. Results and discussion

4.1. Cooling effect and mixture preparation

The cooling effect of EDI is evaluated by comparing the in-cylinder temperature of EDI+GPI (or EDI only) with that of GPI only. Fig. 4 shows the spatial distributions of in-cylinder temperature at different ethanol ratios on a plane cut below the spark plug at spark timing from simulation. The red dot and arrow indicate the position and direction of the EDI injector. As shown in Fig. 4, the charge cooling in the area over the exhaust valve is more effective than that in other areas. This cooling effect becomes stronger with the increase of the ethanol ratio. When the ethanol ratio is greater than or equal to 58%, the near-wall area close to the exhaust valve is over cooled because the temperature is reduced to be lower than 500 K while the mean cylinder temperature is around 690 K. The local overcooling is due to the most concentration of ethanol droplets in this area. In the late compression stroke, the gas velocity becomes low and the ethanol droplets move slowly, causing low heat transfer rate and thus local overcooling. As the ethanol droplets evaporate and absorb the thermal heat from this area, this area has a lower temperature and richer mixture. Such an over-cooled and rich mixture area causes incomplete combustion, and consequently increases the HC and CO emissions.

Although overcooling occurs locally in some regions in cylinder, the overall cooling effect does not increase with ethanol ratio when the ethanol ratio is greater than 58%. As shown in Fig. 5, the predicted mean in-cylinder temperature at spark timing decreases quickly with the increase of ethanol content until the ethanol ratio reaches 58%. However, when the ethanol ratio is greater than 58%, the overall cooling effect of EDI does not increase much. This is because the EDI cooling effect is limited by the low evaporation rate of the ethanol fuel due to its low saturation vapour pressure [15]. Fig. 6 shows the simulated results of the variation of the evaporated/unevaporated ethanol and gasoline fuels with the ethanol ratio by spark timing. With the increase of ethanol ratio, the mean cylinder temperature decreases, leading to reduced evaporation rates for both ethanol and gasoline fuels. The evaporation rate of gasoline drops from 94.3% to 92.0% when the ethanol ratio increases from 0% to 85%. The evaporation rate of ethanol drops from 64.0% to 56.8% when the ethanol ratio increases from 25% to 100%. As a result, the total mass of un-evaporated gasoline and ethanol droplets increases rapidly from 0.873 mg to 9.367 mg when the ethanol ratio increases from 0% to 100%. Higher ethanol ratio has greater cooling potential, but may leave a large number of liquid droplets in the chamber by spark timing. These liquid droplets will keep evaporating during the combustion process and the droplet combustion may occur. This is unfavourable for combustion and leads to high HC and CO emissions.

Since ethanol fuel evaporates slowly in the low temperature environment before the combustion takes place, high ethanol ratio also leads to lean mixture in the combustion chamber. Fig. 7 shows the distributions of the equivalence ratio (*Φ)* around the spark plug by spark timing. The equivalence ratio is defined as follows,

$$\Phi = \frac{Y_e \cdot (O/F)_e + Y_g \cdot (O/F)_g}{Y_{O2}}$$

where Y_e, Y_g and Y_{O2} are the local mass fractions of ethanol, gasoline and oxygen in each cell, $(O/F)_e$ and $(O/F)_g$ are the stoichiometric oxygen/fuel ratios of ethanol and gasoline fuels. As clearly shown in Fig. 7, the equivalence ratio at the plug position decreases with the increase of ethanol ratio. High ethanol ratio (> 58%) does not enhance the overall cooling effect of EDI. On the contrary, it deteriorates the consequent combustion and emission processes. When the ethanol ratio is higher than 58%, the equivalence ratio around the spark plug decreases to be less than 0.5 (0.44 in E76 and 0.37 in E100). Such a lean mixture is out of the ignitable equivalence ratio range of $0.5 < \Phi < 1.5$ [52]. The lean mixture around the spark plug is difficult to be ignited and consequently leads to incomplete combustion and high HC and CO emissions, whose results will be further discussed in Section 4.2.

Moreover, greater ethanol ratio requires longer injection duration of EDI. Longer injection duration enhances the spray penetration and may lead to fuel impingement on the piston and cylinder walls, resulting in increased HC and soot emissions during engine operation [53]. Fig. 8 shows the comparison of the measured and simulated EDI spray patterns at 1.5 ms after the start of injection (ASOI) in a constant volume chamber. The injection pressure was 6 MPa, the ambient temperature was 350 K and the ambient pressure was 1 bar. These conditions reproduced the in-cylinder conditions for an early EDI injection of 300 CAD BTDC in the engine experiments. More information about the spray experiments in the constant volume chamber can be found in [38]. As shown in Fig. 8, the ethanol spray tip penetration reaches 70 mm at 1.5 ms ASOI. The penetration length 70 mm is about the bore diameter (74 mm) and the duration 1.5 ms (equal to 36 CAD at engine speed of 4000 rpm) is close to the EDI injection duration (32 CAD) at ethanol ratio of 46%. Fig. 8 implies that the ethanol fuel impingement may have occurred in engine conditions when ethanol ratio is greater than 46%. Fig. 9 shows the distributions of the ethanol spray droplets at the end of EDI injection at different ethanol ratios in the engine. As shown in Fig. 9, by the end of EDI injection, the ethanol spray tip does not reach the cylinder wall when ethanol ratio is lower than 58%. With the increase of ethanol ratio, the spray penetration length increases and more ethanol droplets reach the cylinder wall, resulting in more wall impingement. This is another factor contributing to the increased HC and CO emissions in the engine experiments, which is shown in Fig. 15.

Higher ethanol ratio requires greater latent heat for fuel evaporation. However, the amount of this cooling potential realised is limited by ethanol's low evaporation rate. More ethanol content needs more energy and time to evaporate, which may lead to incomplete evaporation in the same engine condition. The ethanol ratio and its evaporation are two competing factors that determine the final level of cooling effect and combustion performance: lower ethanol ratio (< 58%) leads to a higher completeness of cooling effect, but limited by its cooling potential; higher ethanol ratio (> 58%) contains more cooling potential, but only a small percentage of it may be realised. Moreover, when the ethanol ratio is higher than 58%, the near-wall area next to the exhaust valve is over-cooled (shown in Fig. 4), the mixture at the spark plug gap is over-lean (shown in Fig. 7) and the fuel impingement on the cylinder wall becomes more significant (shown in Fig. 9). All these cause incomplete combustion and increased CO and HC emissions. When taking the quality of the mixture into consideration, the competing of cooling potential and its evaporation suggests that 40-60% of ethanol ratio can realise the maximum overall cooling effect while avoiding the local overcooling, the too lean mixture at the spark gap and the fuel impingement on the cylinder wall. A similar ratio (30-50%) has been recommended for ethanol/gasoline blends for the conventional single injection engines [5].

4.2. *Combustion characteristics*

To evaluate the combustion characteristics of the EDI+GPI, the in-cylinder pressure, indicated mean effective pressure (IMEP), combustion initiation duration and major combustion duration are discussed. Fig. 10 shows the measured variations of in-cylinder pressure with crank angle degrees at ethanol ratios from 0% to 100%. As shown in Fig. 10, the peak cylinder pressure increases quickly with the increase of ethanol ratio from 0% to 58% and decreases when the ethanol ratio is further increased from 58% to 100%. The in-cylinder pressure with EDI is lower than that of GPI only during the compression stroke (<360 CAD) due to the cooling effect of EDI, leading to less negative work on the piston. During the expansion stroke (>400 CAD), the pressure with EDI is larger than that of GPI only, resulting in more positive work on the piston. Consistently shown in Fig. 11, the IMEP increases quickly when ethanol ratio is in 0%-46% and slowly in 46%-76%, and decreases in 76%-100%.

Fig. 12 shows the combustion initiation duration and the major combustion duration at different ethanol ratios from 0% to 100% derived from the cylinder pressure shown in Fig. 10. The combustion initiation duration, indicated by CA0-10%, is defined as the crank angle degrees from the spark timing to the timing of 10% of the fuel mass fraction burnt (MFB). CA0-10% is directly relates to the combustion stability and only after CA0-10% does flame velocity reach higher values with the corresponding fast rise in cylinder pressure and flame propagation [51]. The major combustion duration, indicated by CA10-90%, is defined as the crank angle degrees from 10% to 90% MFB. The shorter is the CA10-90%, the closer the combustion process is to the constant volume and consequently the higher the thermal efficiency will be [51]. As shown in Fig. 12, the combustion initiation duration decreases with the increase of ethanol ratio from 0% to 58%, indicating an improved combustion stability. However, the CA0-10% starts to increase quickly when the ethanol ratio is higher than 58%. This can be explained by the results shown in Fig. 7. As shown in Fig. 7, the equivalence ratio decreases with the increase of the ethanol ratio. Within 0%-58%, the equivalence ratio is in the ignitable equivalence ratio range of $0.5 < \Phi < 1.5$. The faster flame speed of ethanol fuel contributes to the shorter combustion initiation duration and thus higher combustion stability. However when the ethanol ratio is higher than 58%, the mixture is too lean and out of the ignitable range (Fig. 7) which causes the increased CA0-10%. On the other hand, the major combustion duration decreases quickly with the increase of ethanol ratio from 0% to 58% but slowly from 58% to 76%, and increases when it changes from 76% to EDI only condition.

Fig. 13 shows the flame propagation and distributaions of OH mass fraction at 375 CAD and 395 CAD varying with the ethanol ratios. In premixed combustion modelling, the progress variable *c* is used to indicate the state of the mixture, where c=0 indicates fresh mixture, c=1 is for burnt and 0<c<1 indicates the flame-brush. As shown by the images at 375 CAD in Fig. 13, the mixture burns more quickly in EDI+GPI condition than that in GPI only when ethanol ratio is less than 76%. The flame speed decreases when the ethanol ratio reaches 100%. By the time of 395 CAD, the flame has reached most volume of the combustion chamber. The presence of OH radical is an indicator of the main heat release rate event [54]. Fig. 13 shows that the generation of OH radical is weak at 375 CAD but becomes intensive at 395 CAD. This is consistent with the experimental results shown in Fig. 10, where the cylinder pressure of E100 is smaller in 360-390 CAD but becomes higher after 400 CAD than the pressure of low ethanol ratio conditions. Although EDI+GPI conditions have higher combustion speeds, there are still some unburnt mixture in the near wall region. This is because the ethanol droplets concentrate and evaporate in the near wall region. Fig. 14 shows the distributions of ethanol liquid droplets, equivalence ratio and cylinder temperature at 395 CAD. The ethanol droplets evaporate and absorb thermal heat from the mixture in the near wall region. As a result, this region has a very rich mixture (Φ >2.0) and is over-cooled (< 500 K). The overcooling and over-rich mixture in the near wall region make it hard for the flame to propagate to this region. Consequently, this region has extensive CO and HC emissions as a result of incomplete combustion. On the other hand, the cylinder temperature is much lower in EDI+GPI condition than that in GPI only condition due to the enhanced cooling effect and lean mixture in EDI+GPI. Particularly, the extremely high temperature region (~2500 K) observed in GPI only in Fig. 14 is disappeared when EDI is applied. Following the thermal NOx mechanism of Zeldovich, the NO formation is less significant in EDI+GPI condition. These explain the measured emission values from the EDI+GPI engine tests. As shown in Fig. 15, the measured CO and HC emissions increase, and NO emission decreases with the increase of ethanol ratio from 0% to 100%. Moreover the CO and HC emissions become significantly higher when the ethanol ratio is greater than 58%.

The combustion performance of EDI+GPI engine is improved when implementing EDI within ethanol ratio of 0%-58%. The cylinder pressure and IMEP are increased and the combustion initiation and major combustion durations are decreased when ethanol ratio is increased from 0% to 58%. When further increasing the ethanol ratio from 58% to 100%, the combustion initiation duration and major combustion duration start to increase, while the cylinder pressure decreases, and IMEP increases slightly from 58% to 76% and decreases from 76% to 100%. Regarding the engine emissions, the NO emission decreases when EDI is applied due to the lower combustion temperature and cooling effect. Meanwhile, the HC and CO emissions are increased, and are extremely high at high ethanol ratios (>58%) due to local overcooling and incomplete combustion. Although the engine shows the maximum IMEP at 76%, the exhaust-out CO and HC emissions are very high when ethanol ratio is higher than 58%. The overall cooling effect does not increase with ethanol ratio greater than 58% but leaves a large number of ethanol droplets unevaporated during combustion. Furthermore, over-lean and local overcooling occur, fuel impingement becomes more significant on cylinder wall, and combustion initiation and major combustion durations increase when ethanol ratio is high. Based on comparison of results in all the aspects, the optimal engine performance may exist in the range of ethanol ratio of 40-60% in terms of IMEP, combustion efficiency, cooling effect and emissions.

5. Conclusions

The cooling effect and combustion characteristics of a novel fuel system, ethanol direct injection plus gasoline port injection (EDI+GPI), were numerically and experimentally investigated in a full range of ethanol ratio from 0% (GPI only) to 100% (EDI only). The engine was run at medium load and stoichiometric condition with engine speed of 4000 rpm, spark timing of 15 CAD BTDC and throttle open of 36%. The EDI pressure was 6.0 MPa and the EDI timing was 300 CAD BTDC. The GPI pressure was 0.25 MPa and the GPI timing was 410 CAD BTDC. The main conclusions can be drawn as follows.

1. Compared with GPI only, EDI+GPI demonstrates stronger effect on charge cooling with lower in-cylinder temperature and pressure during the compression stroke. The overall cooling effect increases with the increase of ethanol ratio within 0%-58%. Further increase of ethanol ratio does not increase the overall cooling effect, but leaves a large number of liquid ethanol droplets in the combustion chamber during combustion. Moreover, the local overcooling in the near-wall region and the fuel impingement on the cylinder wall become more significant and the mixture becomes too lean when the ethanol ratio is higher than 58%.

2. The IMEP is increased, and combustion initiation and major combustion durations are decreased when ethanol ratio is in the range of 0%-58%. The combustion performance is deteriorated when the ethanol ratio is greater than 58%, indicated by decreased IMEP and increased combustion initiation and major combustion durations. This is caused by the over-lean mixture around the spark plug, local overcooling and fuel impingement at high ethanol ratio conditions (>58%).
3. The NO emission is decreased with the increase of ethanol ratio due to the enhanced cooling effect and decreased combustion temperature. Meanwhile, the CO and HC emissions are increased with the increase of ethanol ratio due to the incomplete combustion and increased fuel impingement on cylinder wall. The incomplete combustion is caused by the fact that ethanol fuel evaporates slowly in the low temperature environment before combustion, which consequently leaves a large number of liquid ethanol droplets concentrating in the near-wall region, resulting in locally over-cooled and over-rich mixture.
4. The experimental and numerical results showed that the IMEP, thermal efficiency and emission performance of this EDI+GPI engine can be optimized in the range of ethanol ratio of 40-60%, resulted from the effective charge cooling and improved combustion efficiency while avoiding the wall wetting, over-lean and local overcooling issues.

Acknowledgments

The scholarship provided by the China Scholarship Council (CSC) is gratefully appreciated. The authors would like to express their great appreciation to Manildra Group for providing the ethanol fuel.

References

[1] J. Milpied, N. Jeuland, G. Plassat, S. Guichaous, N. Dioc, A. Marchal, P. Schmelzle. Impact of Fuel Properties on the Performances and Knock Behaviour of a Downsized Turbocharged DI SI Engine - Focus on Octane Numbers and Latent Heat of Vaporization. SAE Int. J. Fuels Lubr. 2009; 2: 118-126.

[2] S.M. Shahed, K.-H. Bauer. Parametric Studies of the Impact of Turbocharging on Gasoline Engine Downsizing. SAE Int. J. Engines 2009; 2: 1347-1358.

[3] R.A. Stein, J.E. Anderson, T.J. Wallington. An Overview of the Effects of Ethanol-Gasoline Blends on SI Engine Performance, Fuel Efficiency, and Emissions. SAE Int. J. Engines 2013; 6: 470-487.

[4] N. Fraser, H. Blaxill, G. Lumsden, M. Bassett. Challenges for Increased Efficiency through Gasoline Engine Downsizing. SAE Int. J. Engines 2009; 2: 991-1008.

[5] K. Kar, T. Last, C. Haywood, R. Raine. Measurement of Vapor Pressures and Enthalpies of Vaporization of Gasoline and Ethanol Blends and Their Effects on Mixture Preparation in an SI Engine. SAE Int. J. Fuels Lubr. 2008; 1: 132-144.

[6] P. Price, B. Twiney, R. Stone, K. Kar, H. Walmsley. Particulate and Hydrocarbon Emissions from a Spray Guided Direct Injection Spark Ignition Engine with Oxygenate Fuel Blends. SAE paper 2007-01-0472; 2007.

[7] M. Anbari Attar, M.R. Herfatmanesh, H. Zhao, A. Cairns. Experimental investigation of direct injection charge cooling in optical GDI engine using tracer-based PLIF technique. Experimental Thermal and Fluid Science 2014; 59: 96-108.

[8] K.-h. Ahn, H. Yilmaz, A. Stefanopoulou, L. Jiang. Ethanol Content Estimation in Flex Fuel Direct Injection Engines Using In-Cylinder Pressure Measurements. SAE paper 2010-01-0166; 2010.

[9] L.P. Wyszynski, C.R. Stone, G.T. Kalghatgi. The Volumetric Efficiency of Direct and Port Injection Gasoline Engines with Different Fuels. SAE paper 2002-01-0839; 2002.

[10] E. Kasseris, J. Heywood. Charge Cooling Effects on Knock Limits in SI DI Engines Using Gasoline/Ethanol Blends: Part 1-Quantifying Charge Cooling. SAE paper 2012-01-1275; 2012.

[11] E. Kasseris, J. Heywood. Charge Cooling Effects on Knock Limits in SI DI Engines Using Gasoline/Ethanol Blends: Part 2-Effective Octane Numbers. SAE Int. J. Fuels Lubr. 2012; 5: 844-854.

[12] R.A. Stein, D. Polovina, K. Roth, M. Foster, M. Lynskey, T. Whiting, J.E. Anderson, M.H. Shelby, T.G. Leone, S. VanderGriend. Effect of Heat of Vaporization, Chemical Octane, and Sensitivity on Knock Limit for Ethanol - Gasoline Blends. SAE Int. J. Fuels Lubr. 2012; 5: 823-843.

[13] A.N. Ozsezen, M. Canakci. Performance and combustion characteristics of alcohol–gasoline blends at wide-open throttle. Energy 2011; 36: 2747-2752.

[14] S. Srivastava, H. Schock, F. Jaberi, D.L.S. Hung. Numerical Simulation of a Direct-Injection Spark-Ignition Engine with Different Fuels. SAE paper 2009-01-0325; 2009.

[15] Y. Huang, G. Hong, X. Cheng, R. Huang. Investigation to Charge Cooling Effect of Evaporation of Ethanol Fuel Directly Injected in a Gasoline Port Injection Engine. SAE paper 2013-01-2610; 2013.

[16] R.A. Stein, C.J. House, T.G. Leone. Optimal Use of E85 in a Turbocharged Direct Injection Engine. SAE Int. J. Fuels Lubr. 2009; 2: 670-682.

[17] G. Zhu, D. Hung, H. Schock. Combustion characteristics of a single-cylinder spark ignition gasoline and ethanol dual-fuelled engine. Proc. IMechE Part D: Automobile Engineering 2010; 224: 387-403.

[18] X. Wu, R. Daniel, G. Tian, H. Xu, Z. Huang, D. Richardson. Dual-injection: The flexible, bi-fuel concept for spark-ignition engines fuelled with various gasoline and biofuel blends. Applied Energy 2011; 88: 2305-2314.

[19] R. Daniel, C. Wang, H. Xu, G. Tian, D. Richardson. Dual-Injection as a Knock Mitigation Strategy Using Pure Ethanol and Methanol. SAE Int. J. Fuels Lubr. 2012; 5: 772-784.

[20] C. Jiang, X. Ma, H. Xu, S. Richardson. An Optical Study of DMF and Ethanol Combustion Under Dual-Injection Strategy. SAE paper 2012-01-1237; 2012.

[21] Y. Zhuang, G. Hong. Primary Investigation to Leveraging Effect of Using Ethanol Fuel on Reducing Gasoline Fuel Consumption. Fuel 2013; 105: 425-431.

[22] Y. Zhuang, G. Hong. Effects of direct injection timing of ethanol fuel on engine knock and lean burn in a port injection gasoline engine. Fuel 2014; 135: 27-37.

[23] S.L. Kokjohn, R.M. Hanson, D.A. Splitter, R.D. Reitz. Experiments and Modeling of Dual-Fuel HCCI and PCCI Combustion Using In-Cylinder Fuel Blending. SAE Int. J. Engines 2009; 2: 24-39.

[24] B. Yang, M. Yao, W.K. Cheng, Y. Li, Z. Zheng, S. Li. Experimental and numerical study on different dual-fuel combustion modes fuelled with gasoline and diesel. Applied Energy 2014; 113: 722-733.

[25] C. Abagnale, M.C. Cameretti, L. De Simio, M. Gambino, S. Iannaccone, R. Tuccillo. Combined Numerical-experimental Study of Dual Fuel Diesel Engine. Energy Procedia 2014; 45: 721-730.

[26] M.C. Drake, T.D. Fansler, A.M. Lippert. Stratified-charge combustion: modeling and imaging of a spray-guided direct-injection spark-ignition engine. Proceedings of the Combustion Institute 2005; 30: 2683-2691.

[27] H. An, W. Yang, J. Li, A. Maghbouli, K.J. Chua, S.K. Chou. A numerical modeling on the emission characteristics of a diesel engine fueled by diesel and biodiesel blend fuels. Applied Energy 2014; 130: 458-465.

[28] A. Maghbouli, W. Yang, H. An, J. Li, S.K. Chou, K.J. Chua. An advanced combustion model coupled with detailed chemical reaction mechanism for D.I diesel engine simulation. Applied Energy 2013; 111: 758-770.

[29] V. Knop, A. Benkenida, S. Jay, O. Colin. Modelling of combustion and nitrogen oxide formation in hydrogen-fuelled internal combustion engines within a 3D CFD code. International Journal of Hydrogen Energy 2008; 33: 5083-5097.

[30] B. Franzelli, B. Fiorina, N. Darabiha. A tabulated chemistry method for spray combustion. Proceedings of the Combustion Institute 2013; 34: 1659-1666.

[31] C. Ji, X. Liu, B. Gao, S. Wang, J. Yang. Numerical investigation on the combustion process in a spark-ignited engine fueled with hydrogen–gasoline blends. International Journal of Hydrogen Energy 2013; 38: 11149-11155.

[32] Y. Bai, J. Wang, Z. Wang, S. Shuai. Knocking Suppression by Stratified Stoichiometric Mixture With Two-Zone Homogeneity in a DISI Engine. Journal of Engineering for Gas Turbines and Power 2013; 135: 012803-012801-012803-012809.

[33] D.C. Haworthy, A probability density function/flamelet method for partially premixed turbulent combustion, in: Proceedings of the Summer Program, Center for Turbulence Research, The Pennsylvania State University, 2000.

[34] F. Tap, P. Schapotschnikow. Efficient Combustion Modeling Based on Tabkin® CFD Look-up Tables: A Case Study of a Lifted Diesel Spray Flame. SAE paper 2012-01-0152; 2012.

[35] G. Subramanian, L. Vervisch, F. Ravet. New Developments in Turbulent Combustion Modeling for Engine Design: ECFM-CLEH Combustion Submodel. SAE International 2007-01-0154; 2007.

[36] J.W. Campbell, A.D. Gosman, G. Hardy. Analysis of Premix Flame and Lift-Off in Diesel Spray Combustion using Multi-Dimensional CFD. SAE Int. J. Engines 2008; 1: 571-590.

[37] F. Bazdidi-Tehrani, H. Zeinivand. Presumed PDF modeling of reactive two-phase flow in a three dimensional jet-stabilized model combustor. Energy Conversion and Management 2010; 51: 225-234.

[38] Y. Huang, S. Huang, P. Deng, R. Huang, G. Hong. The Effect of Fuel Temperature on the Ethanol Direct Injection Spray Characteristics of a Multi-hole Injector. SAE Int. J. Fuels Lubr. 2014; 7: 792-802.

[39] S. Henriot, D. Bouyssounnouse, T. Baritaud. Port Fuel Injection and Combustion Simulation of a Racing Engine. SAE paper 2003-01-1845; 2003.

[40] N. Ishikawa, A. Hiraide, T. Takabayashi. Air/Fuel Distribution Simulation in a Port Injected Gasoline Lean-burn Engine. SAE paper 2001-01-1230; 2001.

[41] X. Jiang, G.A. Siamas, K. Jagus, T.G. Karayiannis. Physical Modelling and Advanced Simulations of Gas–liquid Two-phase Jet Flows in Atomization and Sprays. Progress in Energy and Combustion Science 2010; 36: 131-167.

[42] S. Jafarmadar. Three-dimensional modeling and exergy analysis in Combustion Chambers of an indirect injection diesel engine. Fuel 2013; 107: 439-447.

[43] R.D. Reitz. Mechanisms of Atomization Processes in High-Pressure Vaporizing Sprays. Atomization and Spray Technology 1988; 3: 309-337.

[44] A.B. Liu, D. Mather, R.D. Reitz. Modeling the Effects of Drop Drag and Breakup on Fuel Sprays. SAE paper 1993.

[45] ANSYS FLUENT Theory Guide. 2012.

[46] S.S. Sazhin. Advanced models of fuel droplet heating and evaporation. Progress in Energy and Combustion Science 2006; 32: 162-214.

[47] J.M. Duclos, D. Veynante, T. Poinsot. A comparison of flamelet models for premixed turbulent combustion. Combustion and Flame 1993; 95: 101-117.

[48] C. Baumgarten. Mixture Formation in Internal Combustion Engines. Berlin : Springer, c2006; 2006.

[49] G. Stiesch. Modeling engine spray and combustion processes. Springer; 2003.

[50] Y. Huang, G. Hong, R. Huang. Numerical investigation to the dual-fuel spray combustion process in an ethanol direct injection plus gasoline port injection (EDI+GPI) engine. Energy Conversion and Management 2015; 92: 275-286.

[51] W.W. Pulkrabek. Engineering Fundamentals of the Internal Combustion Engine. Prentice-Hall, Inc.; 1997.

[52] H. Li, C. li, X. Ma, P. Tu, H. Xu, S.-J. Shuai, A. Ghafourian. Numerical Study of DMF and Gasoline Spray and Mixture Preparation in a GDI Engine. SAE paper 2013-01-1592; 2013.

[53] A. Matsumoto, W.R. Moore, M.-C. Lai, Y. Zheng, M. Foster, X.-B. Xie, D. Yen, K. Confer, E. Hopkins. Spray Characterization of Ethanol Gasoline Blends and Comparison to a CFD Model for a Gasoline Direct Injector. SAE Int. J. Engines 2010; 3: 402-425.

[54] R.D. Reitz. Directions in internal combustion engine research. Combustion and Flame 2013; 160: 1-8.

Table 1 EDI+GPI engine specifications.

Engine type	Single cylinder, air cooled, four-stroke
Displacement	249.0 cc
Stroke	58.0 mm
Bore	74.0 mm
Connecting rod	102.0 mm
Compression ratio	9.8:1
Intake valve open	22.20 CAD BTDC
Intake valve close	53.80 CAD ABDC
Exhaust valve open	54.60 CAD BBDC
Exhaust valve close	19.30 CAD ATDC
Ethanol delivery system	Direct injection
Gasoline delivery system	Port injection

Table 2 Engine operating conditions.

Ethanol ratio by volume	E0	E25	E46	E58	E69	E76	E85	E100
EDI fuel mass (mg)	-	4.0	8.0	10.7	13.4	15.0	17.3	21.5
GPI fuel mass (mg)	13.4	11.0	8.5	7.0	5.5	4.2	2.7	-

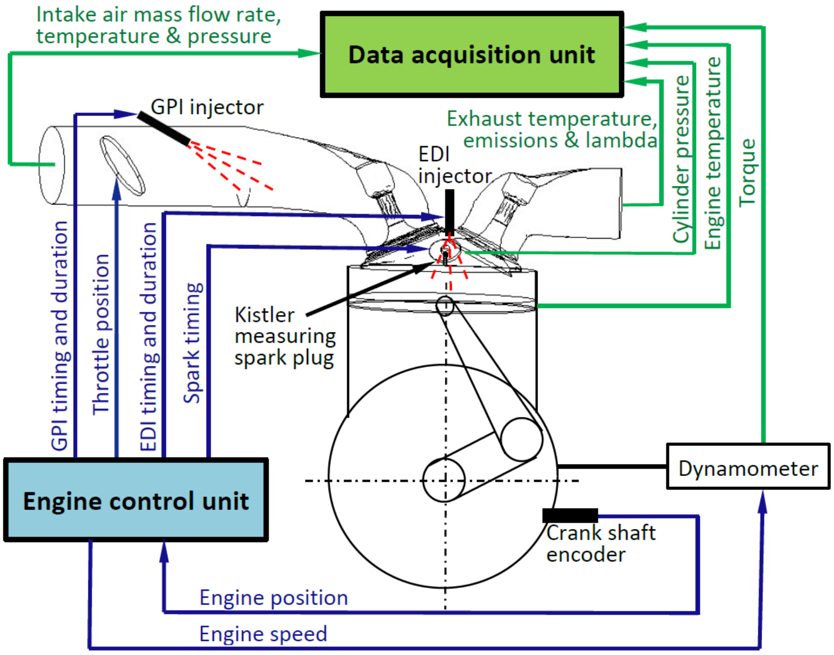

Fig. 1. Schematic of the EDI+GPI engine system. (single column fitting image)

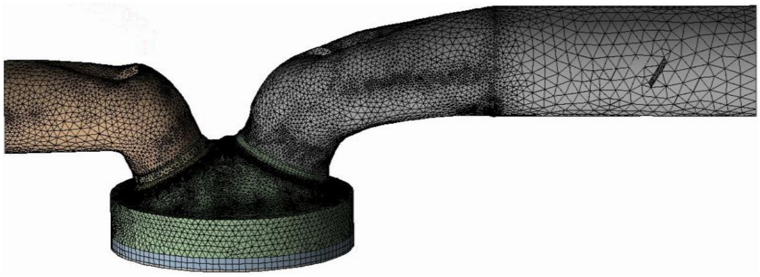

Fig. 2. Computational mesh. (single column fitting image)

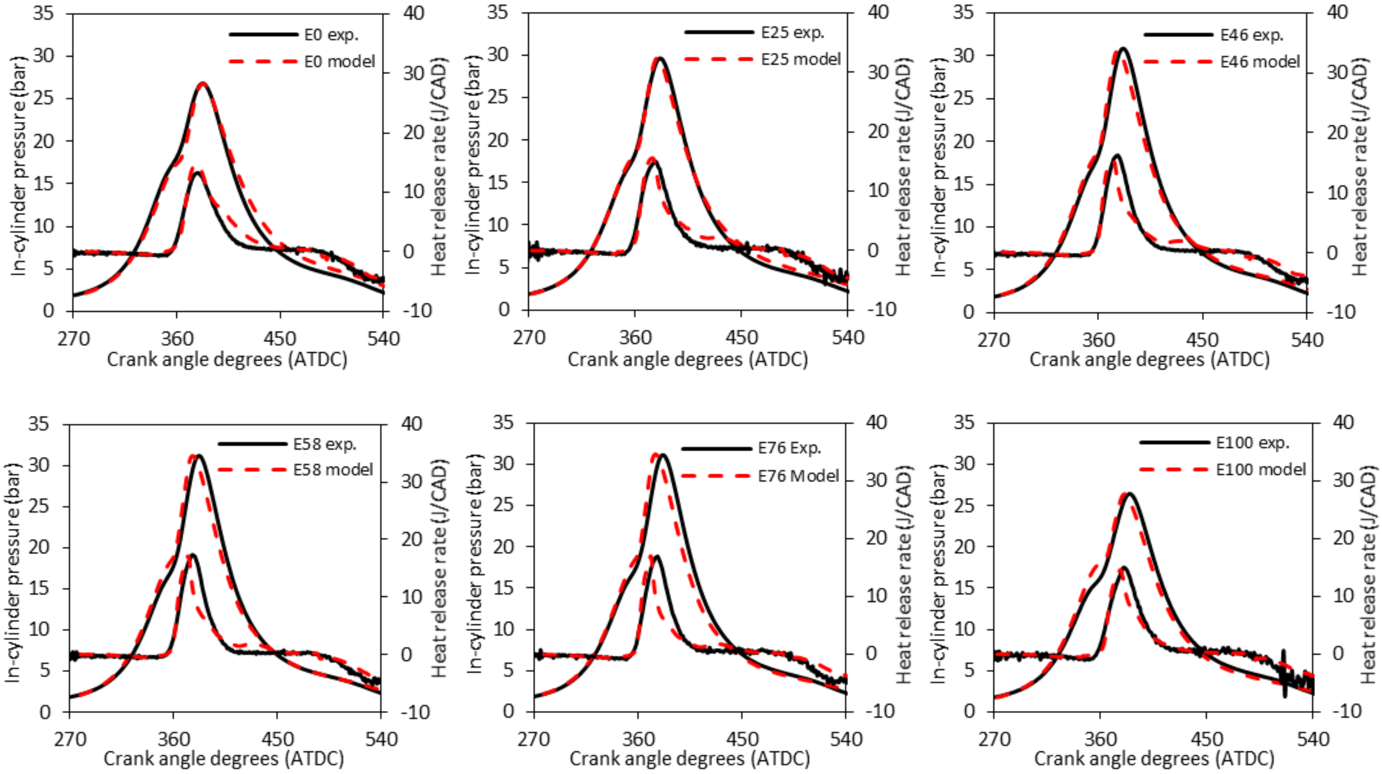

Fig. 3. Comparison between the measured and simulated values of in-cylinder pressure and heat release rate at different ethanol ratios. (2-column fitting image)

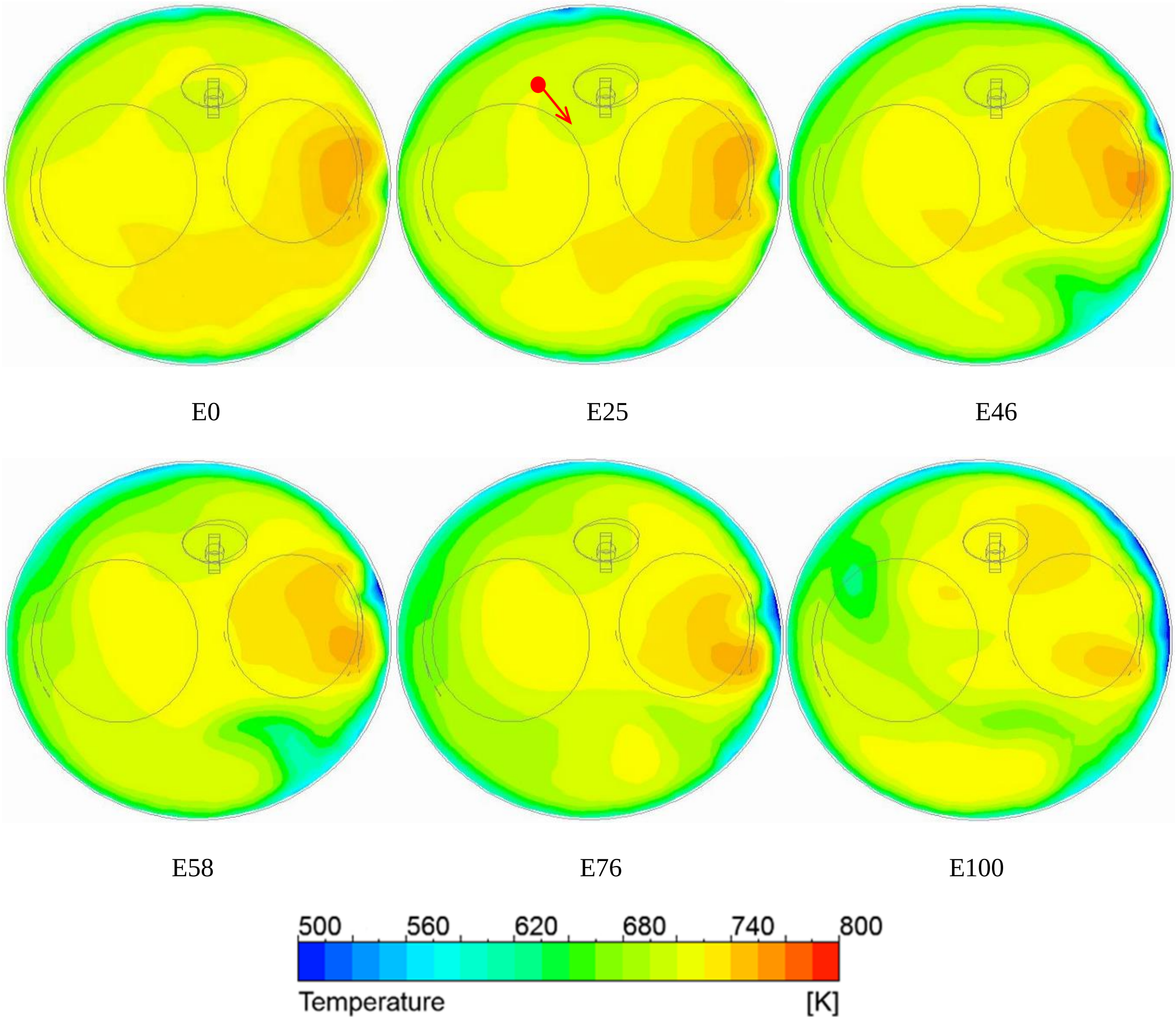

Fig. 4. In-cylinder temperature distributions by spark timing. (2-column fitting image)

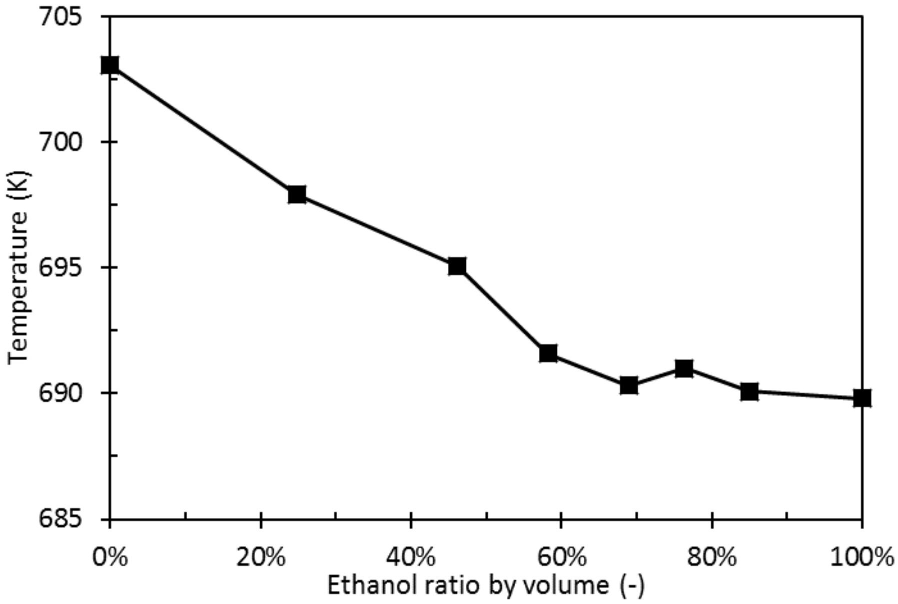

Fig. 5. Variation of mean in-cylinder temperature by spark timing with the ethanol ratios. (single column fitting image)

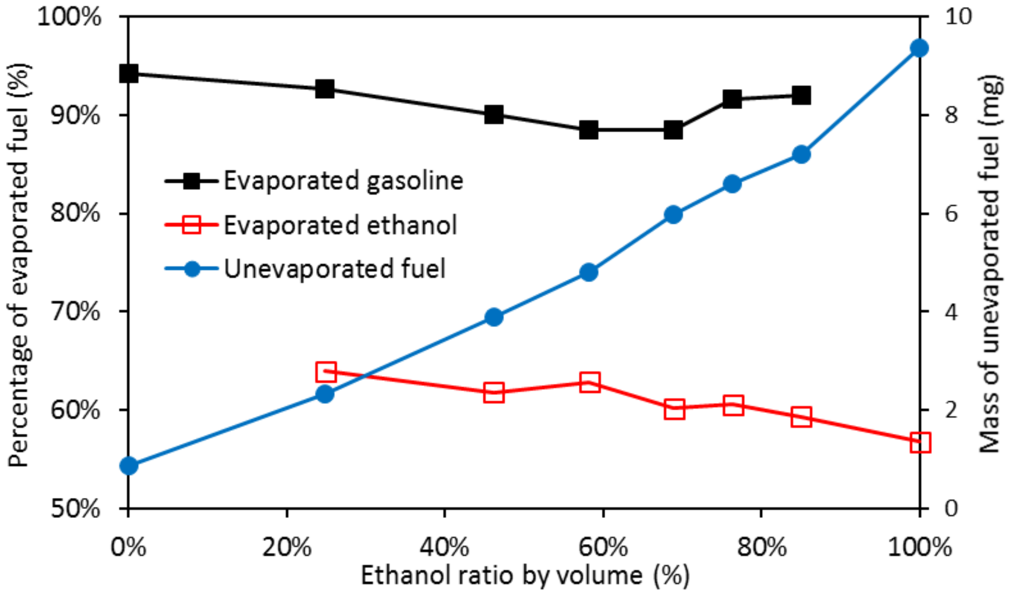

Fig. 6. Completeness of the ethanol and gasoline evaporation by spark timing. (single column fitting image)

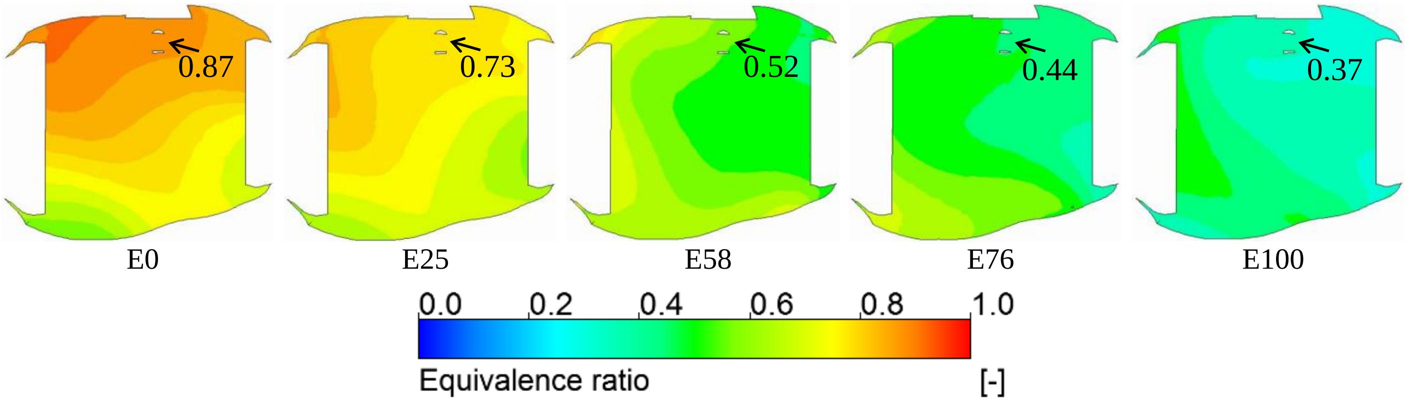

Fig. 7. Distributions of the equivalence ratio around the spark plug by spark timing. (2-column fitting image)

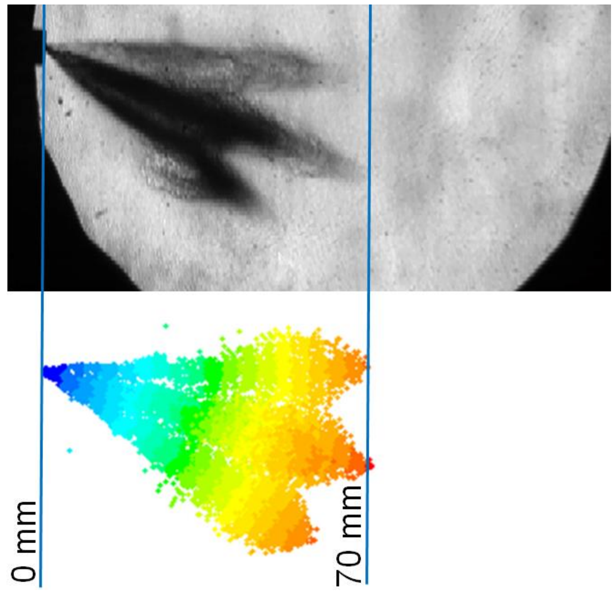

Fig. 8. Comparison of the experimental and numerical results of EDI spray pattern at 1.5 ms ASOI in a constant volume chamber @ 6.0 MPa injection pressure, 1 bar ambient pressure and 350 K ambient temperature [38, 50].

(single column fitting image)

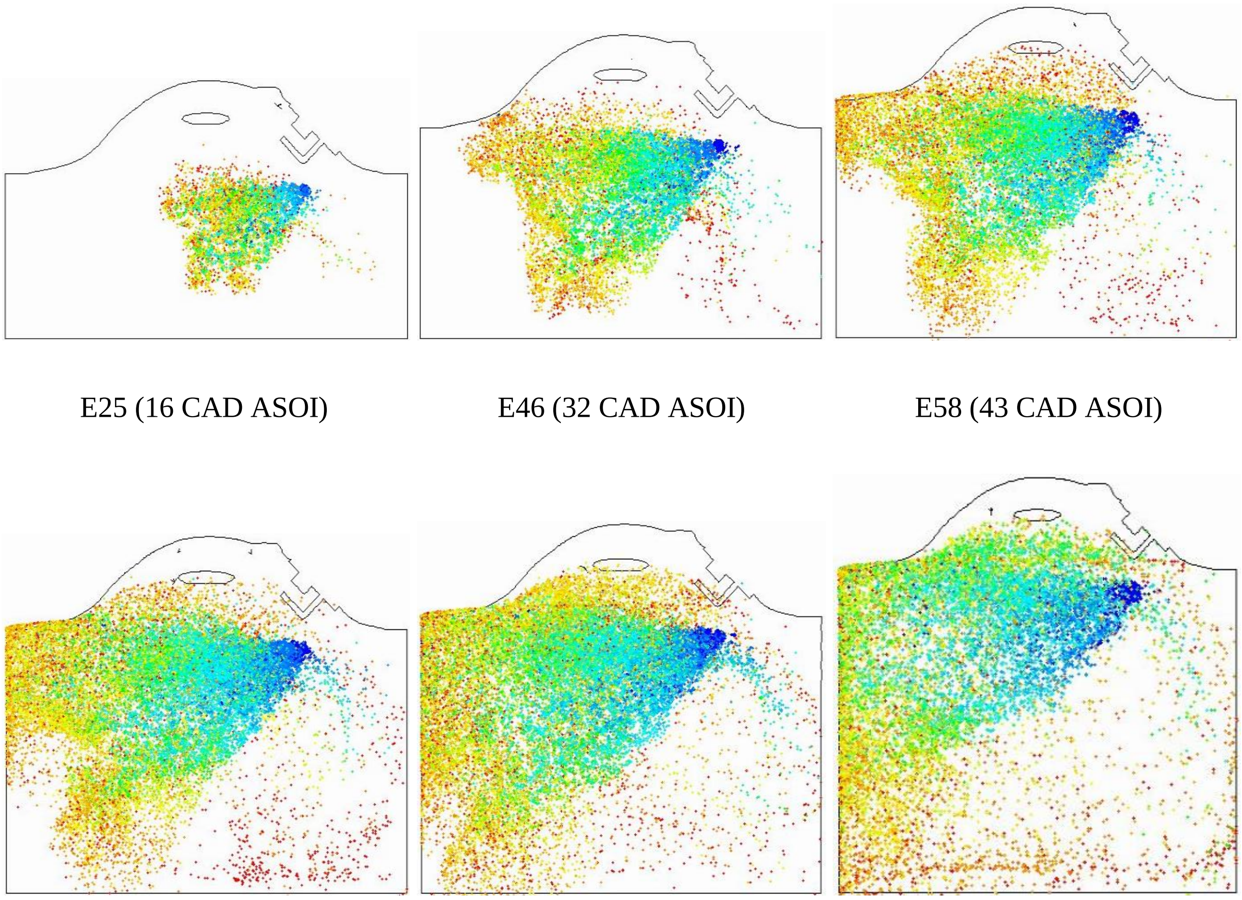

E25 (16 CAD ASOI) E46 (32 CAD ASOI) E58 (43 CAD ASOI)

E69 (54 CAD ASOI) E76 (60 CAD ASOI) E100 (86 CAD ASOI)

Fig. 9. Distributions of the ethanol spray droplets at the end of EDI injection. (2-column fitting image)

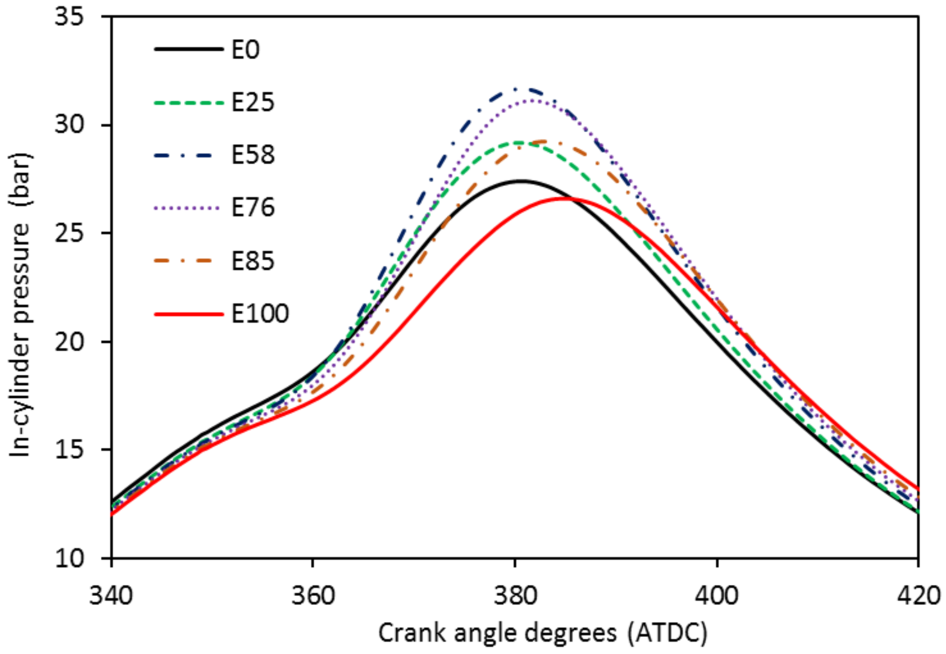

Fig. 10. In-cylinder pressure varying with the ethanol ratios. (single column fitting image)

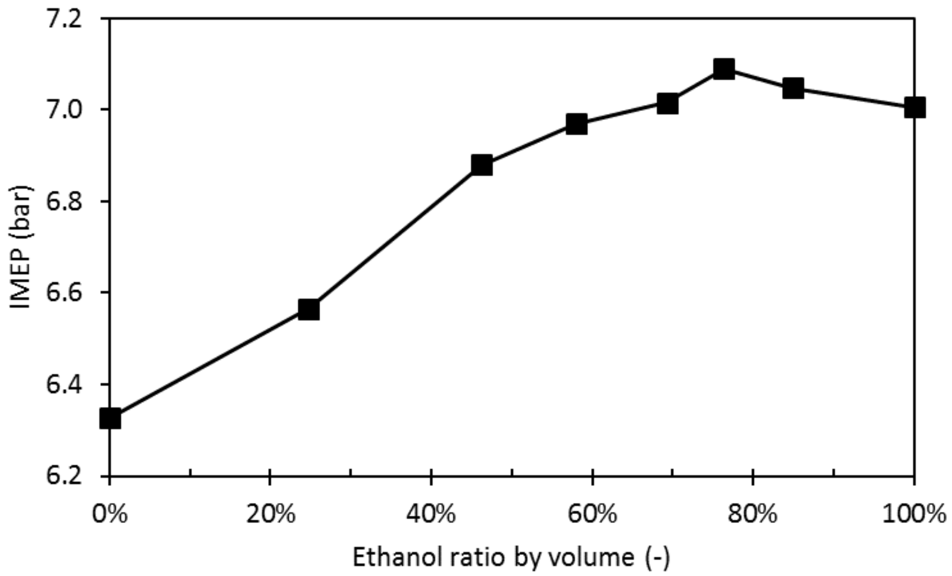

Fig. 11. IMEP varying with the ethanol ratios. (single column fitting image)

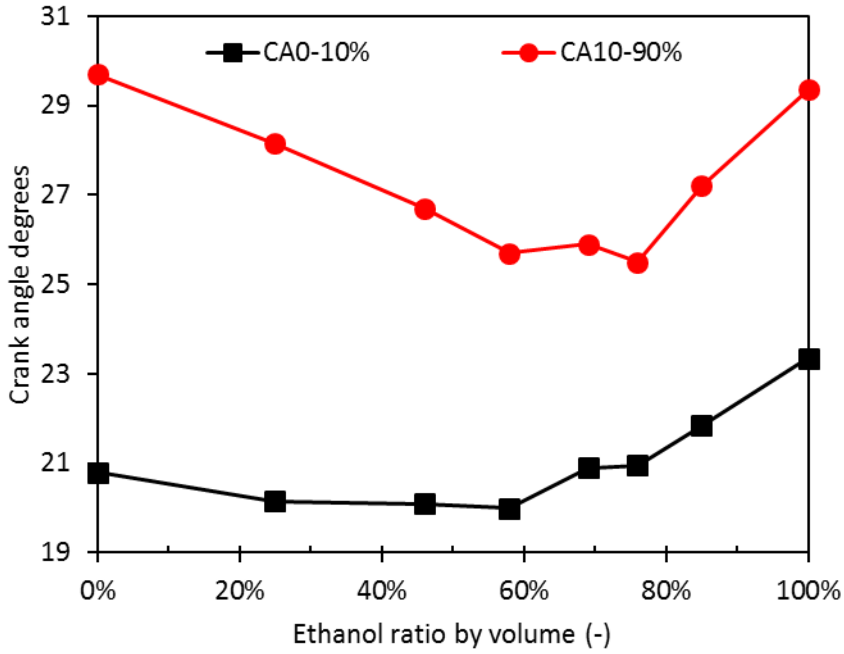

Fig. 12. CA0-10% and CA10-90% varying with the ethanol ratios. (single column fitting image)

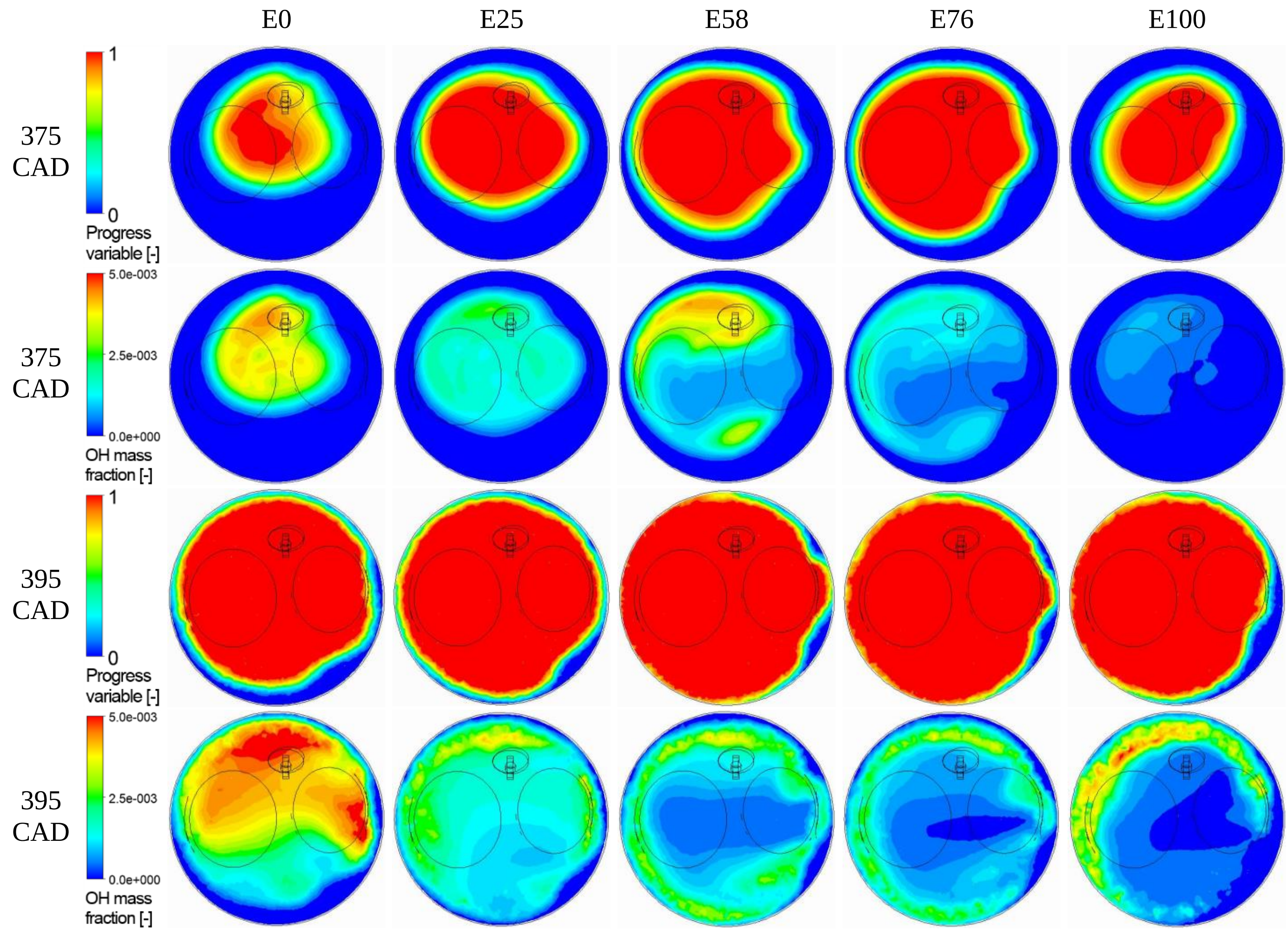

Fig. 13. Flame propagation and distributions of OH mass fraction at 375 CAD and 395 CAD varying with the ethanol ratios. (2-column fitting image)

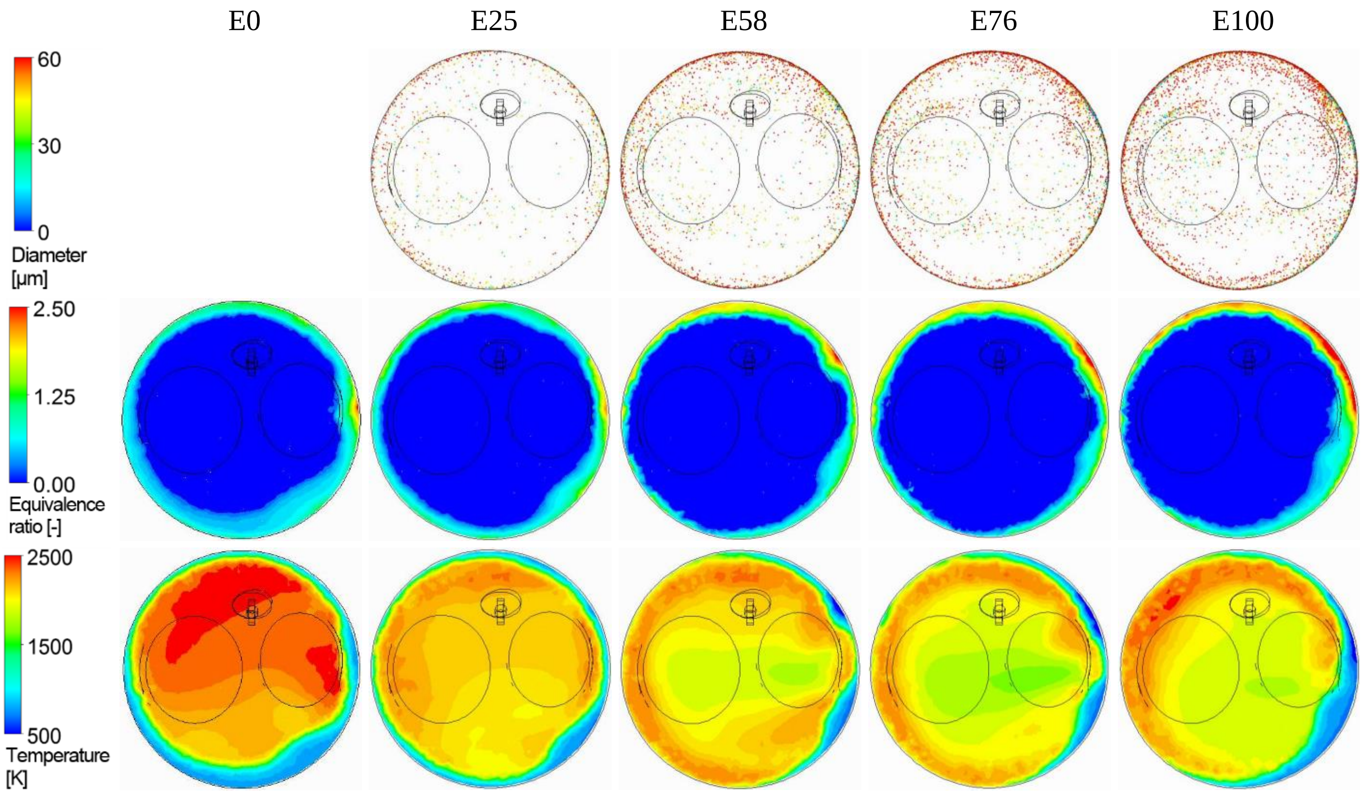

Fig. 14. The distributions of ethanol liquid droplets, equivalence ratio and cylinder temperature at 395 CAD varying with the ethanol ratios. (2-column fitting image)

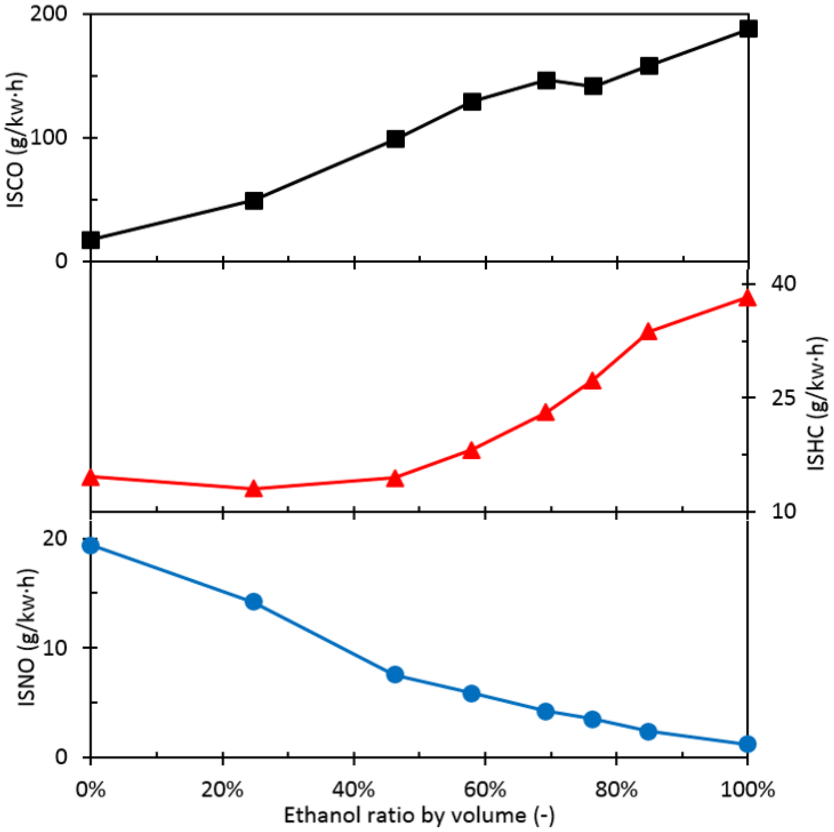

Fig. 15. Measured engine emissions varying with the ethanol ratios. (single column fitting image)